Acta Cryst. (1976). A**32**, 177

On the Nature of Grown-in Defects in Topaz

By P. P. Phakey and R. B. Horney

Department of Physics, Monash University, Clayton, Victoria 3168, *Australia*

(*Received* 16 *July* 1975; *accepted* 31 *August* 1975)

A study has been made of crystals of topaz by optical and interference microscopy, X-ray topography, and scanning and transmission electron microscopy. Most of the samples show a nearly perfect region with dislocation density $\sim 10^2$ cm^{-2} surrounded by a highly defective narrow rim containing dislocations (density $\sim 10^7$ cm^{-2} and higher), low-angle boundaries, networks and planar faults. The Burgers vectors of the dislocations observed in both regions of the crystal have been determined by means of diffraction contrast experiments and the nature of other defects is considered in detail. The relevance of the defects to the anomalous optical properties of the rim is discussed. A direct correlation between etch pits and dislocations in (001) sections of topaz is shown and evidence is presented that screw dislocations or even those with an appreciable screw component are not required for the formation of curl-bottomed pits. The origin of curl-bottomed pits is explained. It is suggested that the sudden increase in the density of dislocations in the rim is due to heterogeneous nucleation of dislocations by local internal stresses in growth layers which have been poisoned by increased impurity concentrations during growth.

1. Introduction

Topaz, $Al_2(SiO_4)(OH,F)_2$, is prized as a semi-precious gemstone. Its crystal structure is orthorhombic with $a=4{\cdot}64$, $b=8{\cdot}78$ and $c=8{\cdot}37$ Å and its space group is *Pbnm* (Alston & West, 1928). Topaz has a perfect (001) cleavage. Its optical properties have been investigated by Rinne (1926) and e.p.r. studies have been reported by Thyer, Quick & Holuj (1967) and Holuj & Quick (1968). The study of grown-in defects in topaz was first made by Gevers (1953) and then by Patel & Goswami (1964) who used the etch-pit technique. The later authors' cleaved (001) sections showed two types of etch pits, the point-bottomed and the curl-bottomed pits. Because a correspondence was observed between the two types of etch pits on upper and lower faces of the cleaved sections, these authors suggested that dislocations were present at the sites of the etch pits. The curl-bottomed pits were supposed to reveal the sites of screw dislocations. Patel & Goswami (1964) also showed that preferential etching of growth layers in topaz occurred giving linear etch grooves from which the inclination of the growth layers was determined. More recently Zarka (1974) made a direct observation of the grown-in dislocations in (001) sections of topaz using the X-ray topographic technique. Dislocations with Burgers vectors along [001], [100], [110], [101] and [111] were reported. An X-ray topographic study of the growth layers in topaz has been carried out by Giacovazzo, Scandale & Zarka (1975).

Although Zarka's (1974) investigation was fairly exhaustive, it only described the nature of defects in (001) sections and it did not relate to the curl-bottomed pits found by Patel & Goswami (1964). When Zarka (1974) published his results we were also engaged in the study of defects in topaz. The present paper reports an investigation of the defects in topaz using the techniques of optical microscopy, interference microscopy, X-ray topography, scanning electron microscopy (SEM) and transmission electron microscopy (TEM). Our observations on (001) sections confirm Burgers vectors of dislocations previously reported by Zarka (1974); they also explain the origin of curl-bottomed pits described by Patel & Goswami (1964). Observations on sections cut parallel to [001] revealed the presence of dislocations with Burgers vector $[01\bar{1}]$ not reported earlier. It is well known that well developed crystals of topaz are surrounded by a narrow rim 0·5 to 1·5 mm thick in which the optical properties are quite anomalous (Rinne, 1926). Except for the results of X-ray work and optical investigation by Rosenberg (1967), very little is known about the rim. The present study reveals that the rim contains a high dislocation density, low-angle boundaries sometimes forming triple junctions, and planar faults. The nature of these defects has been determined from their diffraction contrast effects and it is shown that crystals of topaz have a complex growth history.

2. Experimental

A number of plates parallel to (001), $(1\bar{1}0)$ and (120) were cut from about 15 good quality crystals of Brazilian topaz with shades of colour varying from nearly colourless to light yellow. These plates were polished with alumina powder (5 μm grit size) followed by diamond pads (1 μm particle size) to give a scratch free clear surface. The plates were gently etched in a melt of KOH in a Ni crucible. The final thickness of the plates ranged between 120 and 500 μm. All topographs were taken with Ag $K\alpha$ radiation on Ilford L4 nuclear plates with an emulsion thickness of 50 μm. The μt value of the specimens was always less than 0·3.

For interference and scanning electron microscopy a thin layer of gold was evaporated onto the surface of the plates.

For transmission electron microscopy, doubly polished thin sections of thickness between 30 and 50 μm were prepared by the usual thin-section techniques. Areas of interest in the specimen were then selected using an optical microscope and ultra-thin sections were prepared by ion-beam thinning for examination in a JEM 200 kV electron microscope.

3. Results and discussion

(*a*) *General structure*

Two types of etch pits seen on etched (001) sections of topaz have been described by Patel & Goswami (1964) and Honess (1927). The point-bottomed pits are pyramidal in shape whereas the curl-bottomed pits have a bend in their longer diagonal. For examples see Fig. 6 and 7 of Patel & Goswami (1964). Fig. 1 is a typical example of the appearance of the pits on the etched (001) plates when examined in the SEM. The bend in the longer diagonal of the curl-bottomed pits is fairly angular in shape. In addition to many fine grooves similar to those labelled *GG* in Fig. 1, some broad (and deep) grooves were seen. In these grooves, closely spaced etch pits could be clearly noticed. Since etch grooves are supposed to be due to preferential etching of certain defective growth layers (Patel & Goswami, 1964) it can be suggested that the broad and deep grooves may be due to etching of growth layers where abnormal inpurities were deposited during the growth of the crystal. The presence of these anomalous growth layers can be clearly seen in X-ray topographs which show dark bands and fringes (typical of planar faults) parallel to the prominent growth layers including those marked by etch grooves [see Fig. 2(*a*)].

The impurities responsible for the anomalous growth layers could not be identified unambiguously. The presence of Fe^{3+} impurity at Al^{3+} sites in topaz has been reported (Thyer *et al.*, 1967). All crystals of topaz are also known to have a concentration of F^- up to about 20% by weight (Thyer *et al.*, 1967) and replacement of F^- by OH^- has been demonstrated by the OH absorption peak at 2·745 μm (Holuj & Quick, 1968). Substitution of OH^- for F^- has also been predicted by Rosenberg (1967) from X-ray and optical studies. However, no variations in the concentrations of those elements across growth layers could be detected by the X-ray energy analyser in the SEM. Hence it is possible that the impurity concerned is OH^-. Evans (1964) has shown that OH^- is 12·5% larger than F^-; the replacement of F^- by OH^- would, therefore make the growth layers anomalously strained.

(*b*) *Correlation between etch pits and dislocations*

A correlation between etch pits and dislocations in topaz has been established by Patel & Goswami (1964) by showing a correspondence between etch pits on (i) matched cleavage faces, and (ii) on the opposite sides of a thin plate. When the optical microscope was focused through our plates a similar correlation was observed. X-ray topography revealed that all of the (001) plates considered here contained dislocations (density ~100 lines cm^{-2}) and planar faults characterized by diffraction contrast fringes. The correlation between etch pits and dislocations observed optically in our plates was confirmed by a more direct method described by McDermott & Phakey (1971). Small lead particles were placed at the sites of the etch pits on one side of the plate and X-ray topographs were taken in the usual way making sure that the markers were on the X-ray exit surface of the plate. In Fig. 2(*a*) dislocations are clearly seen to terminate at the white shadows such as *S* of the lead markers.

(*c*) *Burgers vector of dislocations in* (001) *sections*

The characteristics of dislocations in (001) plates were studied in detail by X-ray topography. These plates contained about 100 dislocation lines per cm^2. A typical example can be seen in Fig. 2(*a*) where the $\bar{3}0\bar{3}$ reflexion was used to reduce the contrast from the anomalous growth layers so that the dislocations could be seen more clearly. The orientation of dislocations was determined from the relative positions of their etch pits, the lead-marker technique, from stereographic projections and from stereopair topographs. Although the dislocations in the top half of Fig. 2(*a*) are nearly normal to $(01\bar{1})$ and those in the bottom half are nearly normal to $(0\bar{1}\bar{1})$, variations of up to 15° have been observed. The Burgers vectors of a large majority of these dislocations have been determined from their contrast observed with different reflexions shown in Fig. 3. The dislocations of Fig. 2(*a*) ($\bar{3}0\bar{3}$ reflexion) were also in strong contrast for the $\bar{4}00$ reflexion for $\bar{1}20$ and $\bar{1}10$ reflexions. Dislocation contrast was very weak for 021, 032, 040 [Fig. 2(*b*)] and $0\bar{2}\bar{2}$ reflexions. Accordingly, a large majority of the dislocations seen in Fig. 2(*a*) have a Burgers vector along [100] and their slip planes are of the type {011}. The shortest Burgers vector $\mathbf{b}=a[100]$ agrees with Zarka (1974).

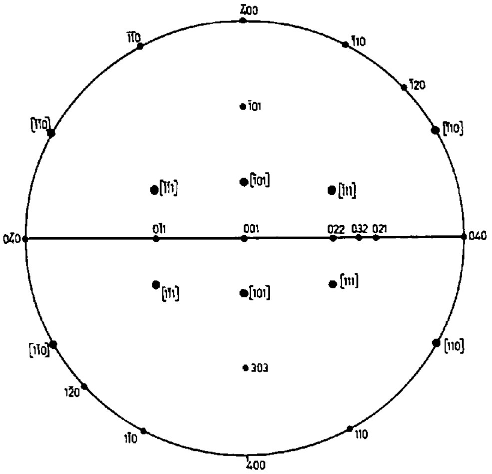

Fig. 3. Stereographic projection of (001) plate showing important reflexions.

(*d*) *Burgers vectors of dislocations in* (120) *and* $(1\bar{1}0)$ *sections*

Fig. 4(*a*) gives a general view of dislocations in a (120) plate where two separate groups are labelled *A* and *B* respectively. All dislocations belonging to group *A* are inclined to the plane of the plate by about 10 to 14°. The trace of their projection is marked in Fig. 5 as *AA*. All dislocations in this group appeared in strong contrast for $1\bar{2}0$, $1\bar{3}0$ and $\bar{3}03$ reflexions, but were almost completely out of contrast for the $\bar{1}2\bar{3}$ reflexion [Fig. 4(*b*)]. Compared with the $\bar{1}2\bar{3}$ reflexion these dislocations were marginally stronger for the $\bar{1}3\bar{3}$ reflexion and weak for $0\bar{2}2$ and $0\bar{2}3$ reflexions. These observations thus suggest that their Burgers vector is along $[\bar{1}11]$. The group *B* includes about six dislocations [Fig. 4(*a*)] inclined to the plane of the plate by an angle of about 12° and they are probably normal to $(1\bar{1}2)$. In Fig. 5, *BB* represents the trace of their projection. With the exception of the one labelled *X* these dislocations were found to be in strong contrast for $02\bar{3}$, $0\bar{2}2$, $\bar{1}3\bar{3}$ and $\bar{1}2\bar{3}$ reflexions, but weaker in $00\bar{6}$ and $1\bar{2}0$ reflexions. They were out of contrast for $0\bar{2}\bar{2}$ and $\bar{4}00$ reflexions [Fig. 4(*c*)]. These observations are consistent with a Burgers vector along $[01\bar{1}]$.

Fig. 6(*a*) shows an example of dislocations in a $(1\bar{1}0)$ plate. The array of dislocations is probably normal to either $(1\bar{2}0)$ or $(1\bar{1}0)$. The dislocations show good contrast in this topograph taken with the $00\bar{6}$ reflexion but they were out of contrast for 120 and 040 reflexions [Fig. 6(*b*)]. Consequently, their Burgers vector must be along [001].

(*e*) *Nature of curl-bottomed pits*

To investigate the nature of the curl-bottomed pits, lead markers were placed at the sites of these pits and X-ray topographs were taken as described previously. Like the point-bottomed pits, dislocations were found to be associated with the curl-bottomed pits. These dislocations were not different from those associated with point-bottomed pits. For example, their orientation was roughly normal to {011} with small variation, their diffraction contrast was similar and their Burgers vector was $\mathbf{b}=a[100]$. Most of the dislocations associated with the curl-bottomed pits were found to be mixed in character with a strong edge component, but some were nearly pure edge; pure-screw dislocations or those with a large screw component were never found. From these observations it is evident that pure-screw dislocations or even those with an appreciable screw component are not required for the formation of curl-bottomed pits as was suggested by Patel & Goswami (1964).

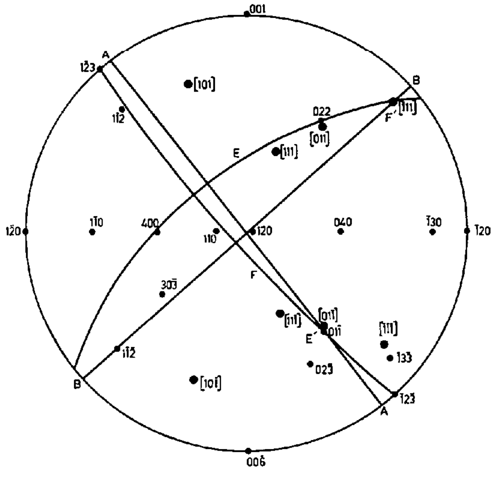

Fig. 5. Stereographic projection of (120) plate.

Close examination of the curl-bottomed pits revealed a short and narrow conical tunnel protruding from the bottom of the pit. In photomicrographs a tunnel appears as a dark line (Fig. 7). On focusing through the crystal it was found that the short tunnel protruding from a pit on the top surface of the section [Fig. 7(*a*)] lined up exactly with a similar tunnel from the corresponding pit on the lower surface [Fig. 7(*b*)]. That is, the tunnels point towards one another like arrows thus providing additional evidence for the correspondence between the curl-bottomed pits on the upper and lower surfaces of the plate. It should be noted that no point-bottomed pit was found to correspond to a curl-bottomed pit.

The conical tunnels are not due to any artefacts of prolonged etching because the depth of the curl-bottomed pits found by interference microscopy was of the order of 7–8 μm which is nearly the same as found by Patel & Goswami (1964). The interferogram also showed that one etch-pit wall continued into the tunnel without a change in its orientation. These results were confirmed by observations taken in the interference-contrast mode in which planes of similar slope have the same colour. On the basis of these observations three-dimensional models of curl-bottomed pits were made (Fig. 8). This figure represents a pair of pits similar to those in Fig. 7.

The conical tunnels are very similar to the etched tracks of high-energy particles in materials (Price & Walker, 1963) but they are associated with dislocations; hence the tunnels must be due to faster preferential dissolution along the dislocation line. Since the images of dislocations connecting the curl-bottomed pits are not noticeably different from other dislocation images it is unlikely that these dislocations have Burgers vectors of unusually large magnitude. However, it is well known that impurities tend to collect along edge dislocations. The conical tunnels can, therefore, arise from preferred dissolution due to the presence of the impurity atmosphere surrounding the edge dislocations. The cause of the non-coincidence of the conical tunnel and the etch-pit bottom is not known. It is possible that the tunnel is asymmetrically etched. Another possible explanation is that the dislocation may have moved slightly from its impurity atmosphere perhaps due to stresses exerted on it during the cutting and cleaving of the plates. If this is the case then during etching dissolution along the dislocation and the impurity atmosphere will simultaneously give a regular etch pit and a tunnel respectively.

(*f*) *Nature of the outer rim of crystals*

Early optical investigations of topaz by Rinne (1926) showed that its (001) sections are always surrounded by a narrow rim in which the optical properties are anomalous. For example, the optic angle $2V$ in the rim varied and was different from that in the main body of the section. He found that the rim could also be seen in (010) sections. This kind of rim was also present in all of our sections which were cut parallel to [001] and the basal sections. However, the thickness of the rim varied from crystal to crystal and was usually between 0·5 and 1·5 mm. Fig. 9(*a*) shows an example of a $(1\bar{1}0)$ section when examined between crossed polarizers. In this figure the outer rim ($\sim$1·5 mm) showing uneven extinction can be seen very clearly. Its X-ray topograph [Fig. 9(*b*)] shows fibrous looking patchy regions of varying intensity and poor resolution. A rim in an (001) section can also be seen in Fig. 2. Ultra-thin sections of the area of interest in the rim seen in Fig. 9, prepared as described in §2, were examined in the electron microscope. It was found that all sections from the rim contained a much higher density ($10^7 \sim 10^8$ cm^{-2}) of nearly straight dislocations than was found in the main body of the crystal by X-ray topography. In addition the rim contained arrays and networks of dislocations. Frequently these dislocation substructures were quite regular, and good examples are shown in Figs. 13, 14 and 16. The dislocation density in Fig. 15 is obviously considerably higher than in Figs. 10 and 13. Fringe patterns indicating planar faults were also a common feature in most areas of the rim. It is therefore clear that although the main body of topaz crystals was nearly perfect with a dislocation density of approximately 100 lines cm^{-2}, the outer rim of the crystals was highly defective. Electron diffraction patterns were taken from a large number of areas in this defective rim. They showed that the defective rim was always a single crystal with orientation nearly the same as in the main body of the crystal. The substructure of the narrow rim is now analyzed.

(*g*) *Analysis of straight dislocations in the rim*

Fig. 10 shows two types of dislocations labelled *A* and *B*. In this figure dislocations of type *A* are nearly out of contrast whereas those of type *B* are in good contrast. The orientation of dislocations of type *A* was determined from stereographic projections following the method described by Nicholson (1968) and it was found that they are aligned normal to $(11\bar{1})$. In addition to the $02\bar{2}$ reflexion (Fig. 10) dislocations of type *A* were also out of contrast for $0\bar{2}1$ and $02\bar{4}$ reflexions. It can be seen from the stereographic projection (Fig. 11) that these observations are consistent with a Burgers vector along [100]. The shortest Burgers vector would be $\mathbf{b}=a[100]$ and this is energetically favourable (Zarka, 1974). The dislocations are of mixed character and their slip plane is $(0\bar{1}1)$.

The straight dislocations seen in Fig. 12(*a*) are in a different area from Fig. 10. Their orientation is different from those described above because they are aligned roughly normal to $(0\bar{2}1)$ or $(0\bar{1}1)$. The dislocations labelled *D* were in contrast for $\bar{1}\bar{3}3$ reflexion (Fig. 12(*a*)) but were found to be out of contrast for the $11\bar{2}$ and $11\bar{3}$ reflexions [Fig. 12(*b*)]. The stereographic projection (Fig. 11) shows that these observations are consistent with a Burgers vector along $[1\bar{1}0]$. These dislocations have, therefore, roughly equal screw and edge components. If the dislocations are normal to $(0\bar{1}1)$ then their slip plane is (111).

(*h*) *Low-angle boundaries*

Diffraction contrast of the array of dislocations shown in Fig. 13(*a*) ($\mathbf{g}=114$) was very similar to that of the straight dislocations with Burgers vector $\mathbf{b}=a[100]$. For example all dislocations in the array were out of contrast for the $02\bar{4}$ reflexion [Fig. 13(*b*)] showing that they also have Burgers vector $\mathbf{b}=a[100]$. The dislocations of this array are nearly pure edge in character and their spacing is approximately $h=2600$ Å which for $|\mathbf{b}|=a=4{\cdot}65$ Å gives an angle of tilt $\theta(=|\mathbf{b}|/h)$ of approximately 6′. Such low-angle tilt boundaries were fairly common in the rim of the crystal. In addition to dislocation arrays, networks of dislocations similar to those seen in Fig. 14 were frequently observed.

(*i*) *Planar faults*

Diffraction-contrast fringes characteristic of planar faults were commonly observed in the rims of the crystals; see Fig. 15(*a*). The trace of their projection indicates that the planar faults are parallel to (011). Topaz crystals suffer damage on prolonged irradiation by electrons in the microscope (Hampar, 1972). Our samples were also found to suffer electron damage,

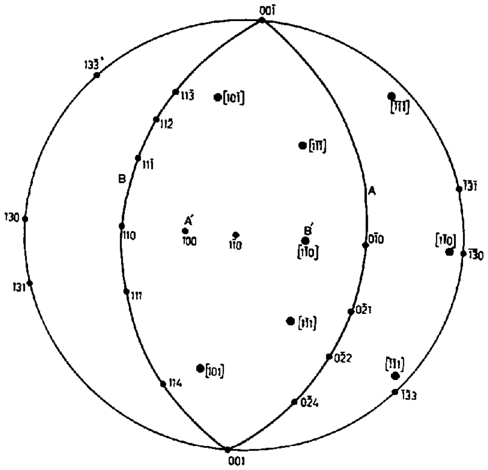

Fig. 11. Stereographic projection of $(1\bar{1}0)$ section showing reflexions relevant to electron microscope observations.

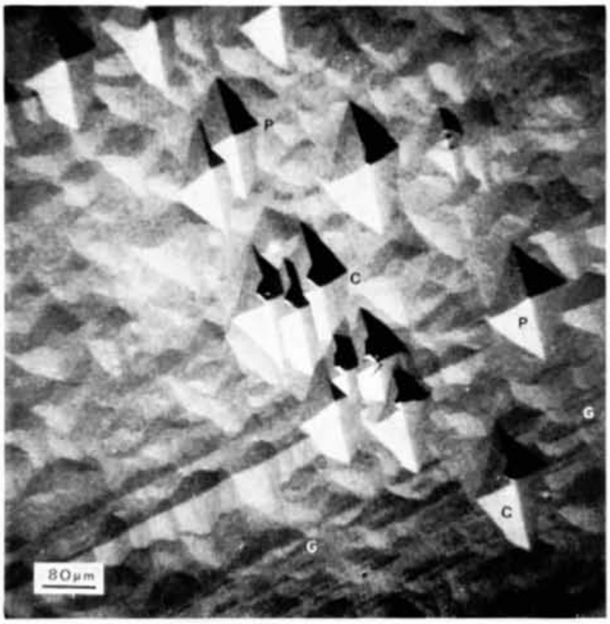

Fig. 1. SEM photograph of etched (001) plate showing point-bottomed pits (*P*), curl-bottomed pits (*C*) and fine grooves *GG*.

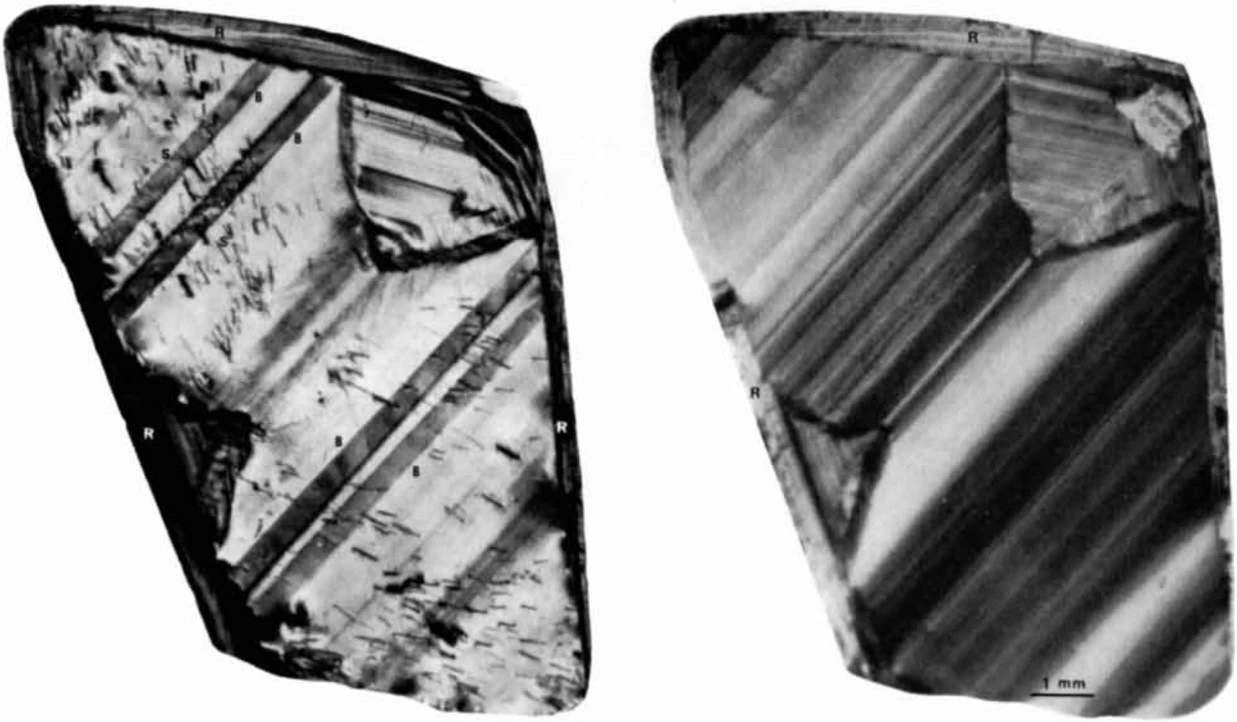

(*a*) (*b*)

Fig. 2. X-ray topographs of (001) plate. (*a*) Dislocations in contrast. $\bar{3}0\bar{3}$ reflexion. Notice white dots (*S*) which are the shadows of the lead markers [see ξ 3(*b*)], dark bands (*B*) and defective rim (*R*). (*b*) Dislocations out of contrast. 040 reflexion.

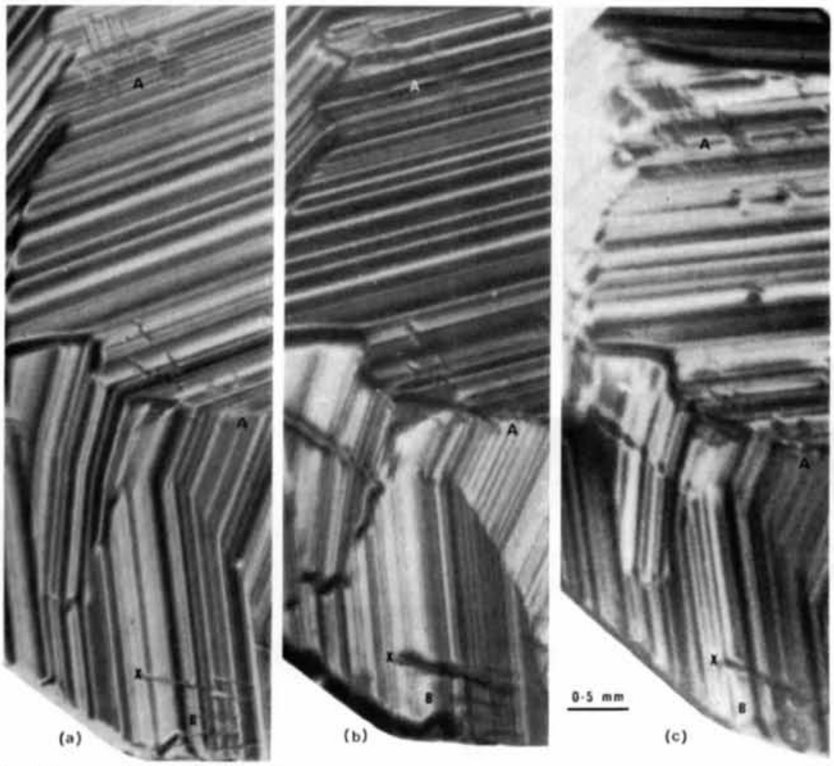

Fig. 4. X-ray topographs of a portion of a (120) plate. Two groups of dislocations labelled *A* and *B*. (*a*) Both groups *A* and *B* in contrast. 006 reflexion. (*b*) Group *A* out of contrast. $\bar{1}23$ reflexion. (*c*) Group *B* out of contrast. $\bar{4}00$ reflexion.

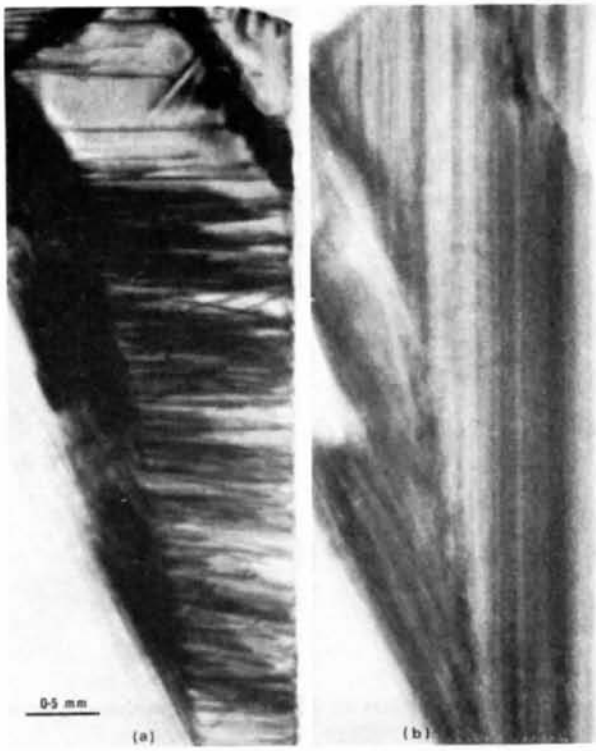

Fig. 6. X-ray topographs of a portion of a $(1\bar{1}0)$ plate. (*a*) Array of straight dislocations in contrast. $00\bar{6}$ reflexion. (*b*) Dislocations out of contrast. 040 reflexion.

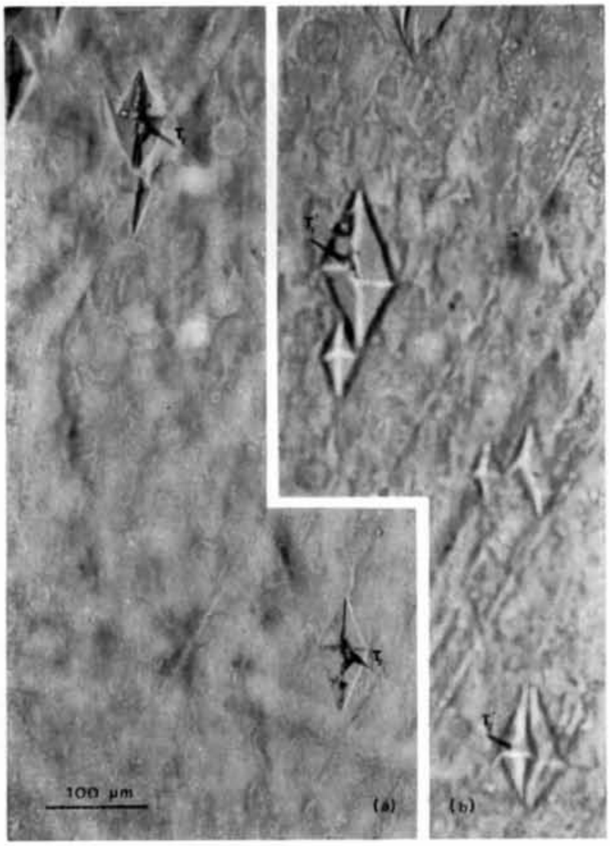

Fig. 7. A synthesized photomicrograph of (001) plate. (*a*) Upper surface in focus. (*b*) Lower surface in focus (viewed through the plate). The conical tunnels T_1 and T_2 on the upper surface correspond to T_1' and T_2' respectively on the lower surface.

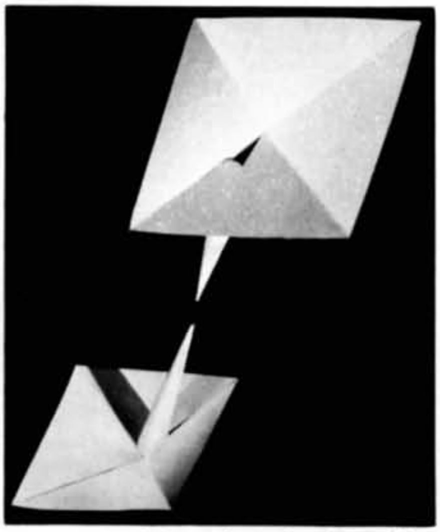

Fig. 8. Photograph of three-dimensional models representing the curl-bottomed pits on upper and lower surfaces of the plate. Compare with Fig. 7. The cones are colinear. Notice the curl in the diagonal of the pit on the upper surface.

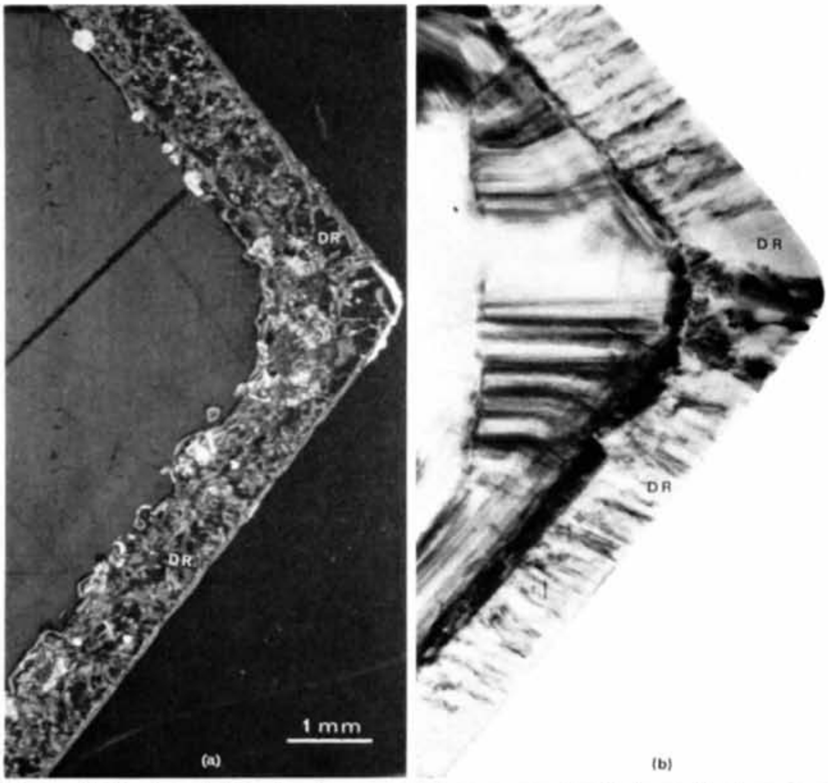

Fig. 9. Defective rim (*DR*) in a $(1\bar{1}0)$ plate. (*a*) Photomicrograph between crossed polarizers. (*b*) X-ray topograph showing same area as (*a*). 120 reflexion. Notice fibrous looking patchy regions.

Fig. 10. Dark-field electron micrograph. Dislocations labelled *A* are out of contrast. $g=02\bar{2}$.

(a) (b)

Fig. 12. Dark-field electron micrographs. Some common dislocations are labelled *B* and *D*. (*a*) $\mathbf{g}=\bar{1}\bar{3}3$. All dislocations are in contrast. (*b*) $\mathbf{g}=11\bar{3}$. Dislocations labelled *D* are out of contrast. Field of view is slightly displaced from (*a*).

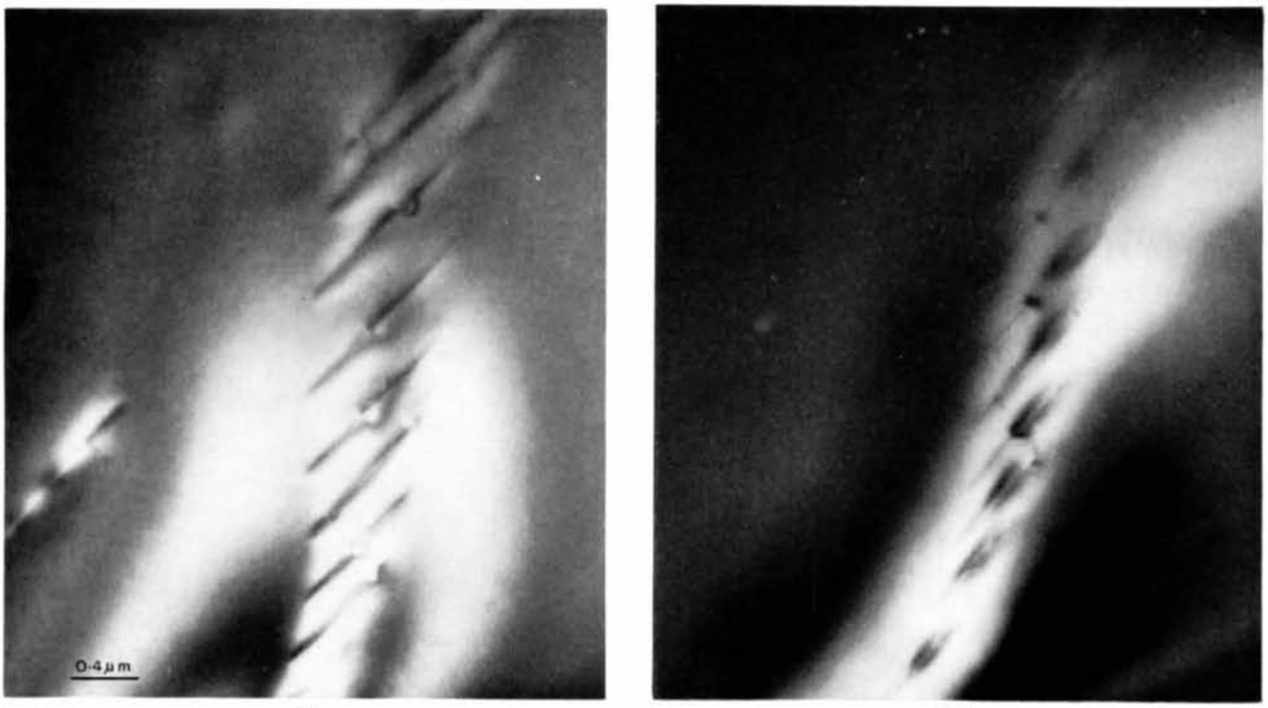

(a) (b)

Fig. 13. An array of nearly pure-edge dislocations of $\mathbf{b}=a[100]$. Dark-field electron micrographs. (*a*) $\mathbf{g}=114$. (*b*) Bend contour for $\mathbf{g}=02\bar{4}$. Array nearly out of contrast.

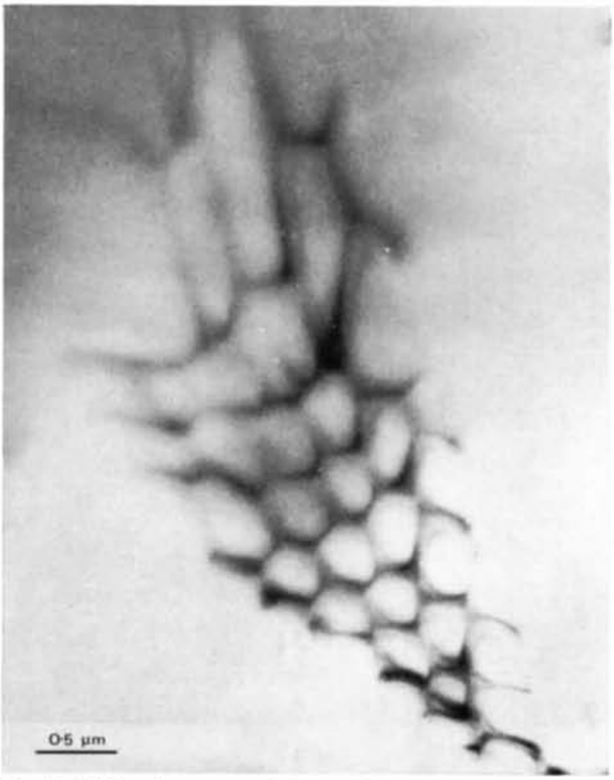

Fig. 14. Dislocation network. Bright-field electron micrograph.

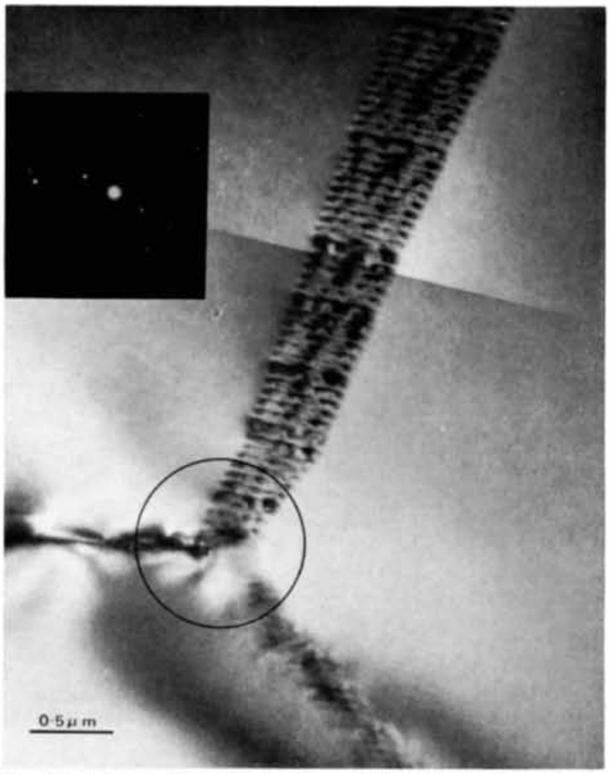

Fig. 16. A triple junction between dislocation arrays. Bright field. The diffraction pattern (from the circled area) shows a single crystal pattern without any noticeable splitting of spots.

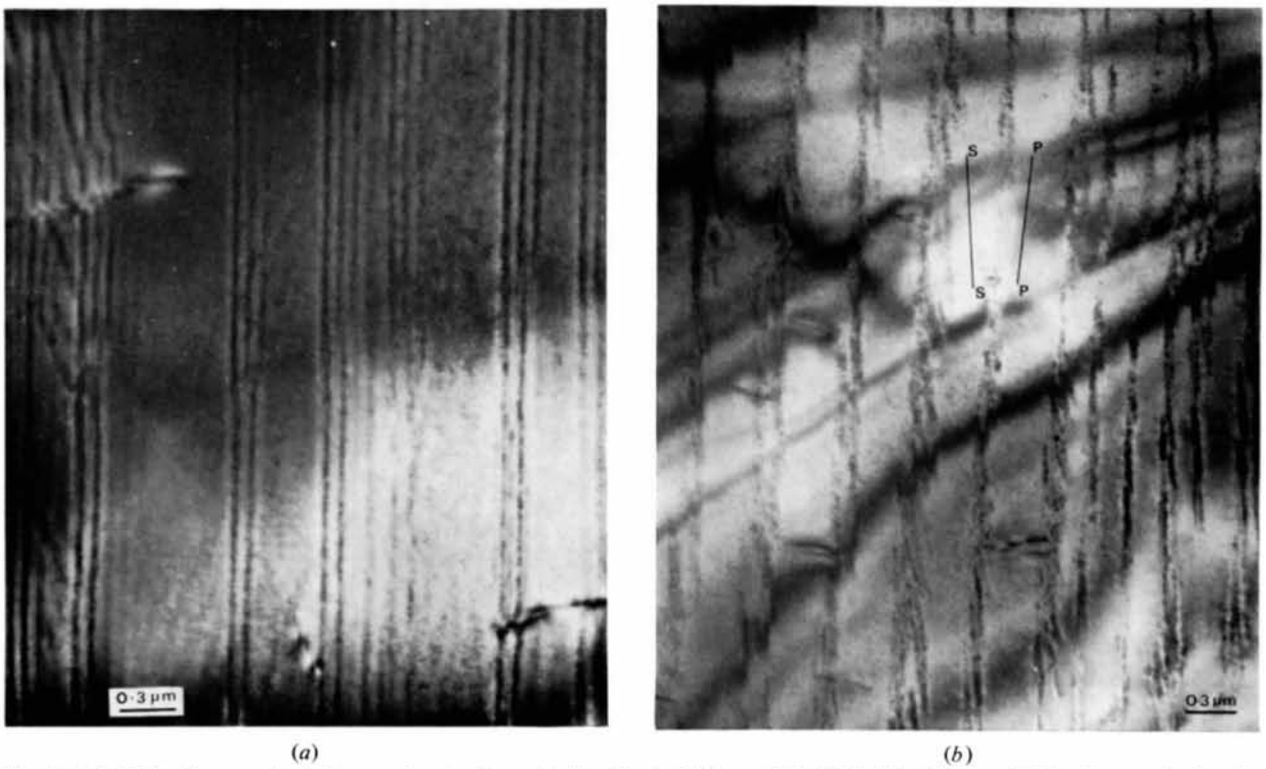

(*a*) (*b*)

Fig. 15. (*a*) Diffraction-contrast fringes due to planar faults. Dark field. $\mathbf{g}=\overline{12}3$. (*b*) Bright-field ($\mathbf{g}=123$) micrograph showing planar faults. Note the discontinuous nature of these faults. *SS* is the trace of shorter segments and *PP* is the trace of (011).

but the damage was more rapid and occurred preferentially along the planar faults; the visibility of the faults was thus unduly enhanced.

The planar faults on (011) were not always continuous but in some cases they were composed of small segments whose plane was different from (011). A good example can be seen in Fig. 15(*b*) where line *PP* represents the trace of (011) and line *SS* the trace of the small segments. The short dislocations seen in Fig. 15 are nearly normal to (011).

Failure to find the true nature of the planar faults is due to the rapid and preferential electron damage along them. There is no convincing evidence to suggest that they are stacking faults introduced in the growth layers to accommodate the impurities because not many of them were found to terminate at partial dislocations as stacking faults do.

Since the F^- content (20% by weight) of topaz can be replaced by OH^- (Rosenberg, 1967; Holuj & Quick, 1968) and the Al^{3+} content can be replaced by Fe^{3+}, it is possible that the planar faults are thin layers of an exsolved phase involving OH^- and/or Fe^{3+}.

(*j*) *Concerning the outer defective rim and growth of crystals*

Our observations have shown that the main body of a topaz crystal is fairly perfect with a low dislocation density typical of undeformed samples. However, the rim surrounding it has a very high density of defects including dislocations, low-angle boundaries, networks and planar faults. Although these defects resemble those commonly found in plastically deformed and recovered materials, it is unlikely that the substructure of the rims is due to plastic deformation as it is only confined to a small volume of material near the external natural faces of the crystals. On the contrary, it appears that the substructure of the rim must be related to its growth.

The principal mechanism for introducing dislocations during growth is heterogeneous nucleation by local internal stresses. High local internal stresses are produced when neighbouring parts of the crystal are constrained to change their specific volume. This can occur when neighbouring regions expand or contract by different amounts due to (i) thermal gradients, (ii) thermal shock, (iii) change in composition, or (iv) change in lattice structure. When the stress reaches a critical value, dislocations are generated.

There is ample evidence to suggest that these processes are operating in crystals of topaz studied by us. The presence of impurities in growth layers of topaz causing changes in *d* spacing is clearly demonstrated by the anomalous growth layers. If the impurity concentration in growth layers is not too large the crystal would keep on growing as a nearly perfect crystal. This is the case in the main body of topaz where many anomalous growth layers and some dislocations are present. However, if the growing faces of a crystal are suddenly poisoned by a large concentration of a certain kind of impurity, the elastic stresses due to processes described above may become so large as to exceed the theoretical shear strength. Dislocations will, therefore, be generated to relieve the elastic strains. If this occurs at high temperatures the dislocations created may react and rearrange forming arrays [Fig. 13(*a*)], networks (Fig. 14), and more complicated arrangements as shown in Fig. 16. Once the growing layers are poisoned and dislocations have been created the growing surfaces become defective and have a high strain energy. Any further growth of the crystal will, therefore, be severely hindered and the crystal may eventually stop growing. The anomalous optical properties of the rim are also most certainly due to the internal elastic strains set up by the defects in it. Such observations are quite common in plastically deformed rocks.

4. Conclusions

1. A direct correlation between etch pits and dislocations in (001) sections of topaz has been established.
2. The grown-in dislocations in topaz are either mixed or pure edge in character. These dislocations have Burgers vectors parallel to [100], [001], $[01\bar{1}]$, $[1\bar{1}0]$ and $[\bar{1}11]$.
3. The relationship between curl-bottomed pits and dislocations has been investigated. Screw dislocations or even those with an appreciable screw component are not required for the formation of curl-bottomed pits. It is shown that curl-bottomed pits result from the preferential dissolution along those dislocations which have a high impurity concentration along them.
4. The narrow rim which surrounds the nearly perfect main body of the crystal and which has anomalous optical properties has a high density of defects such as dislocations, low-angle boundaries, networks and planar faults. These defects have been analyzed.
5. It is suggested that the anomalous optical properties of the rim are due to the internal elastic strains set up by the defects in the rim.
6. It is suggested that when the growth layers of a crystal are suddenly poisoned by a large concentration of impurities, heterogeneous nucleation of dislocations by local internal stresses can occur. The high strain energy associated with the poisoned and defective growth surfaces will hinder further growth of the faces.

Our thanks are due to Professor W. A. Rachinger for his critical comments. We gratefully acknowledge the support of the Australian Research Grants Committee and the Sir Ian Potter Foundation. Messrs R. L. Bryant and P. Batten are thanked for careful photographic work.

References

ALSTON, N. A. & WEST, J. (1928). *Proc. Roy. Soc.* A**121**, 358–367.

EVANS, R. C. (1964). *An Introduction to Crystal Chemistry*. Cambridge Univ. Press.

Gevers, R. (1953). *J. Chim. Phys.* **50**, 321–328.

Giacovazzo, C., Scandale, R. & Zarka, A. (1975). *J. Appl. Cryst.* **8**, 315–324.

Hampar, M. S. (1972). *Proc. 5th International Materials Symposium*, pp. 1256–1266. Berkeley: Univ. of California Press.

Holuj, F. & Quick, S. M. (1968). *Canad. J. Phys.* **46**, 1087–1099.

Honess, A. P. (1927). *The Nature, Origin and Interpretation of the Etch Figures on Crystals.* New York: John Wiley.

McDermott, I. T. & Phakey, P. P. (1971). *J. Appl. Cryst.* **4**, 479–481.

Nicholson, R. B. (1968). *Electron Microscopy and Microanalysis of Metals*, Edited by J. A. Belk & A. L. Davies, pp. 89–120. London: Elsevier.

Patel, A. R. & Goswami, K. N. (1964). *Acta Cryst.* **17**, 569–572.

Price, P. B. & Walker, R. M. (1963). *J. Geophys. Res.* **68**, 4847–4862.

Rinne, F. (1926). *Z. Kristallogr.* **63**, 236–246.

Rosenberg, P. E. (1967). *Amer. Min.* **52**, 1890–1894.

Thyer, J. R., Quick, S. M. & Holuj, F. (1967). *Canad. J. Phys.* **45**, 3597–3610.

Zarka, A. (1974). *J. Appl. Cryst.* **7**, 453–460.

Acta Cryst. (1976). A**32**, 182

Least-Squares Estimates of Equivalent Isotropic Temperature Factors: An Application to H Atoms in Crystalline Sucrose

By Robert F. Stewart

Chemistry Department, Carnegie–Mellon University, 4400 *Fifth Avenue, Pittsburgh, PA* 15213, *U.S.A.*

(*Received* 11 *April* 1975; *accepted* 24 *June* 1975)

An anisotropic harmonic oscillator has mean-square amplitudes of vibration U_1, U_2 and U_3. The geometric mean, $U_{\rm gm}$, is $(U_1U_2U_3)^{1/3}$ and the arithmetic mean $U_{\rm am}$, is $(U_1+U_2+U_3)/3$. It is shown that estimates of $U_{\rm iso}$ which minimize the least-square error of structure factors is bounded by the inequalities $U_{\rm gm} \le U_N \le U_X \le U_{\rm am}$ where U_N is the equivalent isotropic U for the neutron diffraction experiment and U_X is the corresponding estimate of $U_{\rm iso}$ for the X-ray diffraction experiment. The results have been applied to H atoms in sucrose where the U_1, U_2 and U_3 are taken from the neutron diffraction analysis of Brown & Levy [*Acta Cryst.* (1973). B**29**, 790–797]. It is found that $U_X \simeq 0{\cdot}75U_{\rm am}+0{\cdot}25U_{\rm gm}$. When U_X is compared to $U_{\rm iso}$ (X-ray) from Hanson, Sieker & Jensen [*Acta Cryst.* (1973). B**29**, 797–808], U_X's for the fourteen H atoms bonded to C atoms exceed $U_{\rm iso}$ (X-ray) by $\sim 0{\cdot}022$ Å^2 (or equivalently $\sim 1{\cdot}7$ Å^2 in B units, where $B=8\pi^2U$). A systematic trend for the eight hydroxyl hydrogens is not found; the average difference $U_X - U_{\rm iso}$ (X-ray) is $-0{\cdot}006$ Å^2. The discrepancy for H bonded to C is consistent with quantum-chemical calculations of small molecules; the apparent agreement of U_X and $U_{\rm iso}$ (X-ray) for H bonded to O may reflect the influence of hydrogen bonding in crystalline sucrose.

Introduction

It is desirable to compare atomic thermal parameters derived from neutron diffraction data to those obtained from X-ray diffraction analyses. Differences in the results have been interpreted as a deficiency in X-ray atomic form factors (Coppens, 1970). Presumably the charge cloud about the atom is sufficiently deformed by the molecular environment so that thermal parameters from X-ray data are not exclusively a function of the nuclear properties of the molecular crystal. For the case of bonded hydrogen atoms, isotropic temperature factors are spuriously low if free-atom form factors are used (Jensen & Sundaralingam, 1964; Mason, Philips & Robertson, 1965; Hvoslef, 1968). The use of a bonded-hydrogen-atom scattering factor (Stewart, Davidson & Simpson, 1965) generally gives larger thermal parameters.

Hanson, Sieker & Jensen (1973) have reported a detailed comparison of thermal parameters from X-ray and neutron (Brown & Levy, 1973) diffraction analyses of sucrose. In the X-ray refinement, isotropic temperature factors for the H atoms were introduced as least-squares parameters. In the neutron analysis, however, anisotropic temperature parameters were assigned to the protons. The question arises as to what is the equivalent isotropic temperature parameter from the neutron results which is to be compared to the X-ray result. Hanson *et al.* (1973) chose the arithmetic mean of the principal values of the neutron thermal ellipsoid tensor. In an earlier report, however, Hanson, Sieker & Jensen (1972) used the geometrical mean of the three principal values as the equivalent isotropic temperature parameter. Hamilton (1959) has shown that the arithmetic mean corresponds to an isotropic thermal motion with the same value of $\langle r^2\rangle$ as for the anisotropic harmonic oscillator. In the same paper it was acknowledged that this equivalent isotropic thermal parameter does not necessarily minimize the least-squares error. The geometrical mean is determinant-